Reversible adsorption of oxygen as superoxide ion on cerium doped zirconium titanate

Reversible adsorption of oxygen as superoxide ion on cerium doped zirconium titanate.

Valeria Polliotto[a], Stefano Livraghi[a*], Stefano Agnoli[b], Gaetano Granozzi[b], and Elio Giamello[a]
a) Dipartimento di Chimica and NIS, Università di Torino, Via P. Giuria 7, 10125 Torino, Italy.
b) Dipartimento di Chimica, Università di Padova, Via Via Marzolo 1, 35136 Padova, Italy.

Abstract

Zirconium titanate ($ZrTiO_4$) modified via cerium ions insertion in the oxide lattice has been successfully prepared via Sol-Gel synthesis forming solid solutions in the molar range between 0 and 10%. Cerium ions are hosted both as Ce^{4+} and Ce^{3+} ions whose ratio depends on the treatment undergone by the solid, with trivalent cerium always abundantly present even in strong oxidative conditions. Surface exposed Ce^{3+} ions are capable to adsorb O_2 in the range of temperature between 273K and 77K, as superoxide anion ($O_2^{\bullet-}$), having side-on structure and characterized by complete surface-to-molecule electron transfer (about 98% of spin density on O_2 molecule). Surprisingly such abundant adsorption is pressure dependent and fully reversible opening the perspective of applications of this system in the field of oxygen separation from gas mixtures.

Keywords:

EPR, XPS, $ZrTiO_4$, Cerium, Superoxide, reversible adsorption

1 INTRODUCTION

The superoxide species ($O_2^{\bullet-}$) represents a key species in many chemical processes ranging from the catalysis to the biochemistry. In heterogeneous photocatalysis the $O_2^{\bullet-}$ anion is an intermediate of paramount importance since it can directly react with target substrates or it can evolves to H_2O_2 which represents a powerful oxidizing agent.[1] In selective oxidation processes based on Mars–van Krevelen mechanism, the $O_2^{\bullet-}$ formation and its evolution to peroxide species is also a crucial step occurring on the surface of the catalysts where surface oxygen atoms, removed by reaction with the target molecules, are subsequently replenished by reaction with O_2 from the gas phase.[2-4] The superoxide anion is also involved in the reversible absorption of oxygen occurring on both inorganic or biological systems, a process of high importance in different research areas such as the oxygen transport in biological systems or the field of selective adsorption and separation of gas mixtures.[5,6] Some examples of such substrates in biochemistry are for instance the hemoglobin, the myoglobin or the hemocyanin. In all these examples the oxygen molecule is coordinated to a metal centre as iron or copper.[7,8] The reversible oxygen absorption is also reported for some inorganic systems, and also in this second case, the interaction of the oxygen molecule with a transition metal centre (usually host by an organic framework) plays a crucial role. In almost of the cases the absorption mechanism involves charge transfer between the metal centre and the oxygen with the oxidation of the metal and the simultaneously reduction of the oxygen molecule to superoxide ($O_2^{\bullet-}$).[7] Formation of peroxo-adducts is also reported.[9,10]

A prominent role in the coordination of oxygen is played by cobalt compounds. For instance, the fact that aqueous ammonia solutions of cobalt(II) are able to reversibly bind molecular oxygen was already reported in nineteenth century and further characterization has been done in the following years.[7,10,11] More recent examples involve Co(II) ions encapsulated in zeolite[12] or metal-organic frameworks[13-15]. In spite of the different nature of all these chemical systems, the mechanism involved is mostly the same. Cobalt (II) is oxidized to Co(III) and the oxygen is reduced to the superoxide form according to the process $Co^{2+} + O_2 \leftrightarrows Co^{3+}–O_2^{\bullet-}$.

The same mechanism is also invoked for systems involving other metals centres, for instance chromium,[16] manganese[8] or iron[17] even though, in some cases, not necessarily with a complete electron exchange to give a metal-superoxide adduct.[18]

Reversible O_2 absorption was also observed on metal oxides. CoO-MgO solid solution reversibly adsorbs oxygen via an electron transfer mechanism analogous to that reported for the Co complexes.[19,20] Other metal oxides, for which reversible oxygen absorption is reported, are CeO_2, In_2O_3 and the CeO_2-TiO_2 mixed oxide. In the case of CeO_2-TiO_2 mixed oxides the origin of the reversible O_2 adsorption was ascribed to the presence of Ce^{3+} centres in the $Ce_2Ti_2O_7$ pyrochloric phase present at the interface of the two oxides and formed along the synthesis of the material.[21] In the other two examples (CeO_2 and In_2O_3) the superoxide adduct formation was ascribed to electron transfer processes involving trapped electrons in the defects of the solids. [22-24] During a thorough investigation of wide band gap semiconducting oxides doped with Ce ions we have prepared Ce-doped zirconium titanate ($ZrTiO_4$). This is a monophasic solid containing Ce ions diluted in the $ZrTiO_4$ matrix (scrutinyite structure), that shows an abundant reversible adsorption of dioxygen at the surface. Here we report the investigation of the basic features of this phenomenon mainly performed by electron paramagnetic resonance (EPR). Work is in progress in our laboratory to explore at deeper level the quantitative aspects of the interaction and the possible applications of this material in the area of gas mixtures separation.

2 EXPERIMENTAL

2.1 Samples preparation.

The pristine $ZrTiO_4$ powder (hereafter ZT) was prepared via the sol−gel technique, mixing a solution of 3.5 ml of titanium(IV) isopropoxide and 5 ml of zirconium(IV) propoxide (molar ratio 1:1) in 9 ml of 2-propanol and adding 3.5 ml of water. The gel was left to age for 15 hours at 290 K and subsequently dried at 343 K. The dried material was calcined in air at 973 K for 1 hour. The powder

presented a white color. Ce doped-$ZrTiO_4$ powders (hereafter Cex-ZT where x is the Ce molar ratio) powders were prepared in a similar manner, mixing a solution of 3.5 ml of titanium(IV) isopropoxide and 5 ml of zirconium(IV) propoxide (molar ratio 1:1) in 9 ml of 2-propanol to which 3.5 ml of water solution of $CeCl_3 \cdot 7H_2O$ was added in order to have different molar ratio of cerium (from 0.5 mol% to 10 mol%). The gel was left to age for 15 hours at 290 K and subsequently dried at 343 K. The dried materials were calcined in air at 973 K for 1 hour. Oxygen absorption test were carried out on the samples at the two edge of the loading range (0.5 mol% and 10 mol%).

2.2 O_2 adsorption.

O_2 absorption was carried out after an activation process performed in order to get rid of all contaminants adsorbed on the surface according to the following procedure. An initial thermal annealing in vacuum at 773K for 30 minutes was followed by an oxidation step again at 773K for 60 minutes under 20 mbar of O_2. The surface adsorption of O_2 was investigated in three distinct experiments in order to check all possible interactions occurring between this molecule and the modified oxide.

1) Dosing of O_2 in the range of temperature between room temperature and 77K.

2) Dosing of O_2 with the sample kept under UV light irradiation at liquid nitrogen temperature (77 K). For the investigation a 1600 W Xenon lamp (Oriel instruments) with a light beam output set at 1000W and equipped with a IR water filter was used. In such condition photoreduction occurs.[25]

3) Dosing of O_2 on the sample previously annealed at 573K in vacuum (residual pressure $P < 10^{-3}$ mbar). In a such a way a further amount of excess electrons in the material due to lattice oxygen depletion upon vacuum annealing can reduce the oxygen.[25]

2.3 Materials characterization.

Powder X-ray diffraction (XRD) patterns were recorded with a PANalytical PW3040/60 X'Pert PRO MPD diffractometer using a copper Kα radiation source and the X'Pert High-Score software was used for data handling. Diffraction patterns were refined with Rietveld method using MAUD (Material Analysis Using Diffraction) program.[26,27]. The surface area measurement was carried out on a

Micromeritics ASAP 2020/2010 apparatus using the Brunauer–Emmett–Teller (BET) model for N_2 adsorption measurements. Prior to the adsorption run, the sample was outgassed at 573 K for 2 hours. Continuous Wave Electron Paramagnetic Resonance (CW-EPR) experiments were performed with a Bruker EMX spectrometer operating at X-band (9.5 GHz), equipped with a cylindrical cavity operating at 100 kHz field modulation. All the spectra were recorded with a Modulation Amplitude of 0.2 mT. Spectra at 77K were obtained keeping the sample in liquid nitrogen using a finger Dewar set in the EPR cavity. For the spectra recorded in the range 130 K – 300K A variable temperature unit was employed to record spectra at different temperature intervals. Spectra under irradiation were recorded "in situ", directly illuminating the sample, kept at 77 K in liquid nitrogen, inside the EPR cavity using a 1600 W Newport Xe lamp.

For the X-ray photoemission spectroscopy (XPS) measurements, the oxide powers were suspended in MilliQ water, sonicated for 15 minutes and drop casted on gold coated aluminum supports. The resulting thin film samples were introduced into the load lock of an ultra-high-vacuum (UHV) system and left outgassing overnight at a base pressure lower than $5x10^{-7}$ mbar. Then photoemission measurements were taken in the main chamber of the ultra-high-vacuum system at a base pressure of $5•10^{-9}$ mbar at room temperature, by using an Omicron DAR 400 x-ray source (Al Kα=1486.7 eV) and a VG Mk II Escalab electron analyzer.

A homogeneous charging was observed, therefore the binding energy (BE) scale was adjusted using the adventitious carbon signal and setting its position to 284.8 eV. After the XPS measurements, the samples were subjected to an annealing process at 550 °C in UHV and then to an oxygen treatment at 400°C in 5 mbar O_2 (purity 5.0) for 30 minutes and then transferred back to the analysis chamber, without any air exposure, for further measurements, under UHV conditions. The photoemission lines were analyzed using the XPSPEAK 4.1 software, which uses a mixed linear and Shirley background, and symmetrical Gaussian-Lorentzian functions.

3. Results and discussion.

$ZrTiO_4$, zirconium titanate, is a semiconducting oxide mid-way, in composition, between TiO_2 and ZrO_2. The two parent oxides interact with cerium in opposite manner. Zirconia, fluorite structure, can dilute Ce^{4+} ions in the lattice in substitutional position forming solid solutions.[28] The solubility of Ce^{4+} in the lattice of ZrO_2 is favoured by the fact that both ZrO_2 and CeO_2 show fluorite structure. Differently, in the case of TiO_2 where the structure of all its polymorphs is based on linked TiO_6 octahedra, which is clearly different from that of cerium oxide. Ce ions cannot be simply diluted in the TiO_2 matrix but, rather, upon reaction at high temperature, CeO_2 and TiO_2 form a new phase ($Ce_2Ti_2O_7$) having the pyrochlore structure.[21]

Zirconium titanate has a structure analogous to that of titania polymorphs being based on edge sharing and corner sharing MO_6 (M= Zr^{4+} or Ti^{4+}) units giving rise to the scrutinyite structure, typical of α-PbO_2. Surprisingly, $ZrTiO_4$ that, in structural terms, is more similar to TiO_2 than to ZrO_2 is capable to host Ce ions (in a range between 0 and 10% of molar fraction investigated in this work) in the positions of the cationic sub lattice causing a progressive modification of the lattice parameters of the solid as recently reported.[29] Detailed analysis of the XRD data can be found in the supplementary information (Figure S1 and S2) where it is shown that when the concentration of Ce reaches the limit of 10 mol% a small fraction of ZrO_2 phase is segregated.

Table 1 summarizes the main features of the two samples studied, in the present work, for the experiments of O_2 absorption test.

Sample	Ce loading (mol%)	$ZrTiO_4$ (%w/w)	ZrO_2 (%w/w)	Crystal size $ZrTiO_4$ (nm)	Crystal size ZrO_2 (nm)	R(%)	Surface area BET (m^2/g)	$Ce(III)/Ce_{tot}$ (at%) XPS
Ce05-ZT	0.5	100	-	20±0.2	-	5.4	61	48
Ce10-ZT	10	95	5	18±2.3	16±2.6	5.8	72	42

Table 1: Phase composition, crystallites size and surface oxidation state of the as prepared Ce doped $ZrTiO_4$ samples employed in this work, evaluated via Rietveld refinement of the XRD patterns, BET and XPS.

3.1 XPS characterisation.

XPS was employed to monitor the oxidation state of cerium in the as prepared samples and its evolution along the activation procedure (see experimental section) by reproducing the procedure in situ.

Ce 3d XPS data for the as prepared Ce-doped $ZrTiO_4$ samples are reported in Table 1 (last column). The atomic percentage of Ce(III) species has been determined using a standard multipeak analysis, and dividing the chemically shifter component pertaining to Ce(III) (i.e. the v',v° multiplet, *vide infra*) by the total intensity of the Ce 3d photoemission line. After the described calcination and before any further thermal treatment, both samples show the presence of a relevant amount of Ce(III). This indicates that after the synthesis, even though the last step of the preparation consists of an oxidation treatment at high temperature, only a fraction of the total cerium is present with the maximum oxidation number. The presence of Ce(III) in the oxidic matrix needs an electrostatic compensation. The most probable healing process is not simply related to the presence of electron holes, but implies oxygen vacancies (V_O), with one vacancy every two Ce^{3+} ions, to compensate the charge unbalance effects due to Ce^{3+}. The resulting solid involving the two forms of cerium (Ce^{4+} and Ce^{3+}) can be described in the following way and assuming that the Ce ions take preferentially the position of Zr^{4+} in the lattice because of the similar size.

$$Ce_x^{3+}Ce_y^{4+}Zr_{(1-x-y)}^{4+}O_{(2-x/2)}^{2-}(V_O)_{x/2}$$

Further XPS experiments on the Ce10-ZT sample show that the oxidation state of cerium can be easily modified by thermal treatments under UHV conditions or in an oxygen atmosphere (Figure 1). Following the classical approach of Burrows [30-32], the Ce 3d photoemission spectrum can be separated into two doublets related to Ce (III) (v',v°) and Ce(IV) (v,v'',v'''). After the annealing at 550°C in UHV, a strong reduction is observed and the fraction of Ce(III) reaches 84%. On the other hand, exposing the sample to oxidising condition (high temperature in presence of O_2, see experimental section) this value drops to 25%. Zirconium titanate, as the parent oxides TiO_2 and, at

much lesser extent, ZrO_2, lose oxygen upon annealing under vacuum with consequent formation of excess electrons in the solid which, in the bare $ZrTiO_4$ material, reduce the Ti^{4+} or the Zr^{4+} cations.[25] On the contrary, in the Ce10-ZT sample, beside to the described change of the cerium oxidation state, only negligible changes are observed in the Zr 3d and Ti 2p core level levels, indicating that the redox chemistry of the materials is mostly ruled by the cerium species, even if they are present in a smaller amount. The following reaction describes the above mentioned redox process.

$$O^{2-}_{Lattice} + 2Ce^{4+} \rightleftarrows \tfrac{1}{2}\, O_2 + V_O + 2Ce^{4+} + 2e^- \rightleftarrows \tfrac{1}{2}\, O_2 + V_O + 2Ce^{3+} \qquad (1)$$

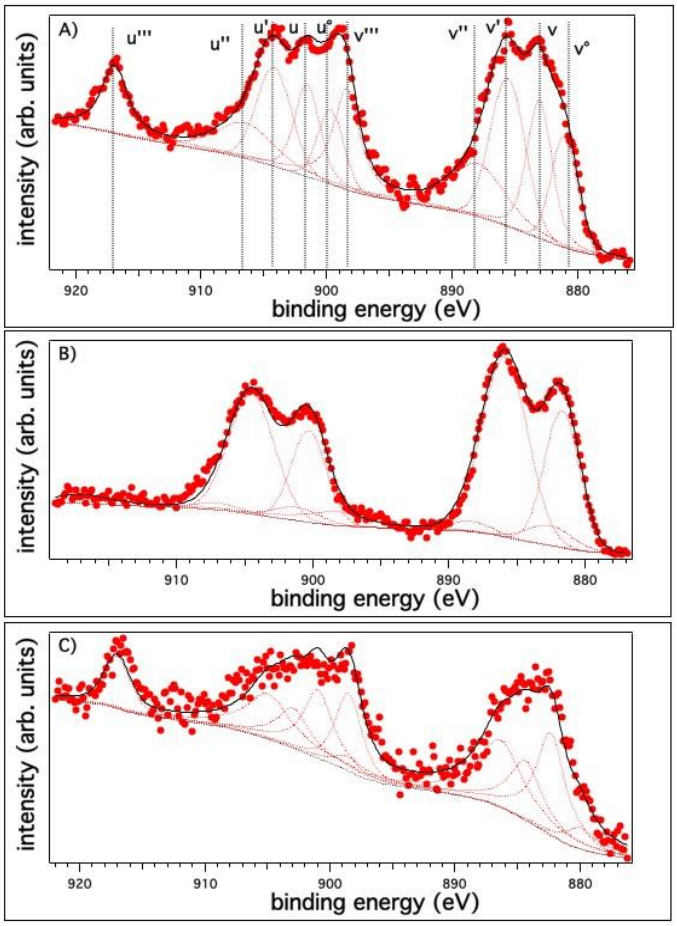

Figure 1: Ce 3d XPS data of Ce10-ZT sample. A) as prepared, B) annealed at 550 °C in UHV, C) oxidized at 400°C in O_2.

Figure 2 shows that during the sample treatments the O 1s XPS data also present a remarkable evolution. In the as prepared material, the oxygen photoemission line comprises three peaks, a main component centred at 530.3 eV ascribed to the lattice oxygen in the solid solution,[33] and two other components at 531.8 eV and 533.3 eV that can be associated with hydroxyl species and adsorbed

water, respectively.[34,35] It is worth mentioning, that in this same binding energy range (530.5 eV 532.2 eV) also superoxide and peroxide species have been documented on ceria, however their stable existence is connected to the presence of an oxygen partial pressure as demonstrated by *in operando* near ambient pressure photoemission measurements.[36] After annealing under UHV conditions at 550°C for 30 minutes, the O 1s spectrum become sharper: all the water is desorbed, and only the peaks related to lattice oxygen and hydroxyl species, even though quite reduced in intensity, can be observed. After the exposure to oxygen (30' at 400°C in 5 mbar O_2), the O 1s spectrum becomes broader especially on the low BE side. Here a new component centred at 529.3 eV and related to loosely bound oxygen species defects can be clearly identified.[37]. It is worth mentioning that these species are quite labile and tends to decrease as a function of time under x-ray exposure.

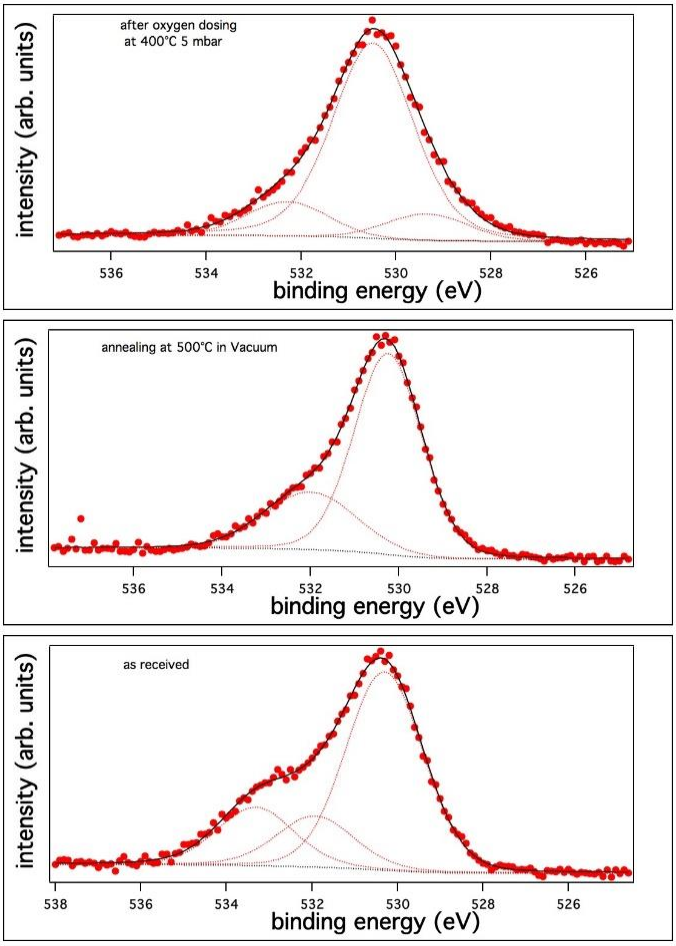

Figure 2: O 1s XPS data of Ce10-ZT sample. A) as prepared, B) annealed at 550 °C in UHV, C) oxidized at 400°C in O_2.

Summarizing, the XPS data show that Ce-doped $ZrTiO_4$ samples contain a large amount of Ce(III) and also after an "in situ" oxidation the Ce(III) is still abundantly present at the surface of the samples.

The thermal treatment in oxygen slightly affects the amount of surface OH groups and simultaneously generates a new family of oxygen related surface sites. Despite an obvious change of the Ce oxidation state (Ce(III) vs Ce(IV)) due to the external conditions, the fact remains that the solids prepared in this work contain a substantial concentration of Ce(III) in any circumstance.

3.2 EPR Evidence of the reversible formation of the $O_2^{\bullet-}$ species.

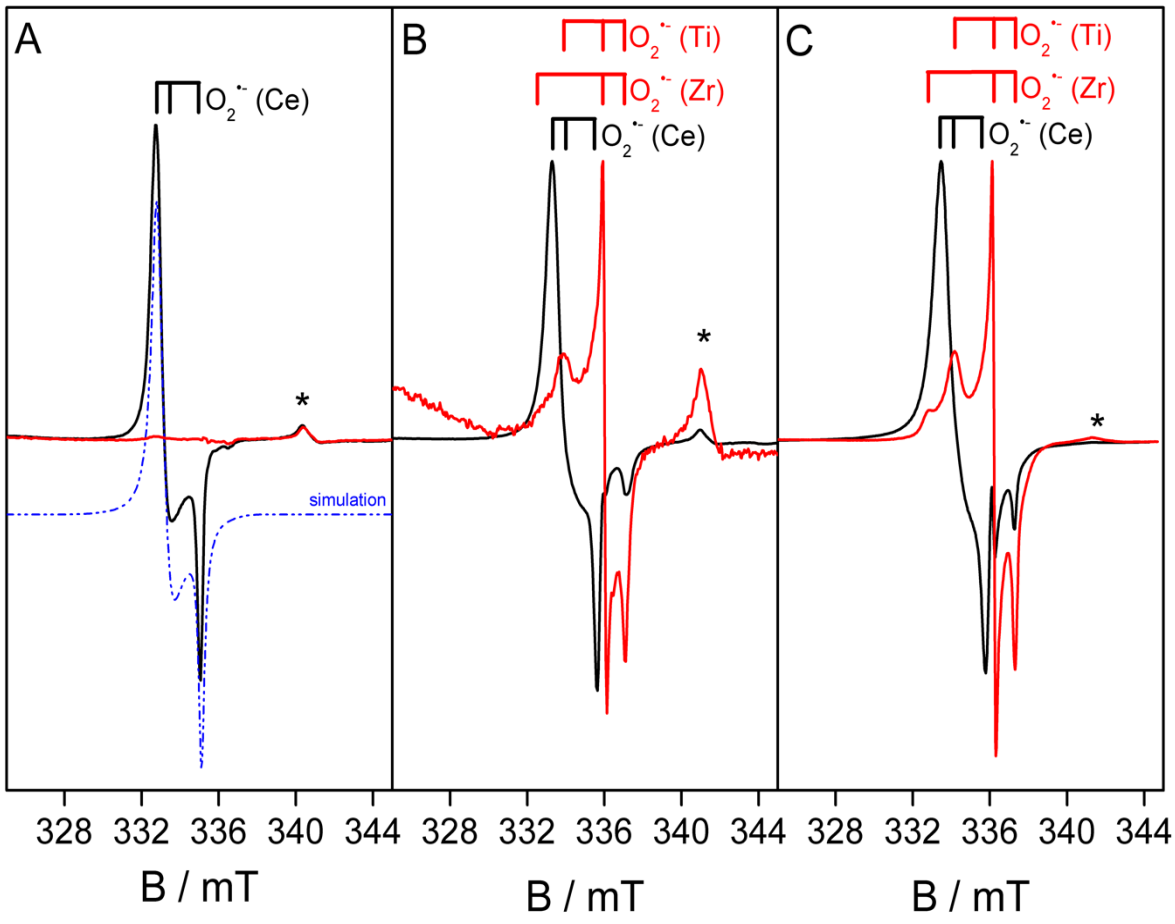

Figure 3: Normalized EPR spectra in presence of 2 mbar of O_2 (black spectra) and after O_2 outgassing (red spectra). Panel A: Activated Ce05-ZT. The blue dot-dashed curve is the computer simulation of the signal obtained in presence of O_2. Panel B: Activated Ce05-ZT irradiated with UV-visible light in presence of O_2. Panel C: Thermally annealed Ce05-ZT contacted with O_2. All Spectra were recorded at 77 K with a microwave power of 10 mW. Due to the relevant difference in intensity the spectral intensity was normalized for a better comparison. The red trace actually corresponds to an intensity that is about two order of magnitude lower than that of the black line signal. The asterisk indicates the Zr^{3+} signal always observed in $ZrTiO_4$ based compound.

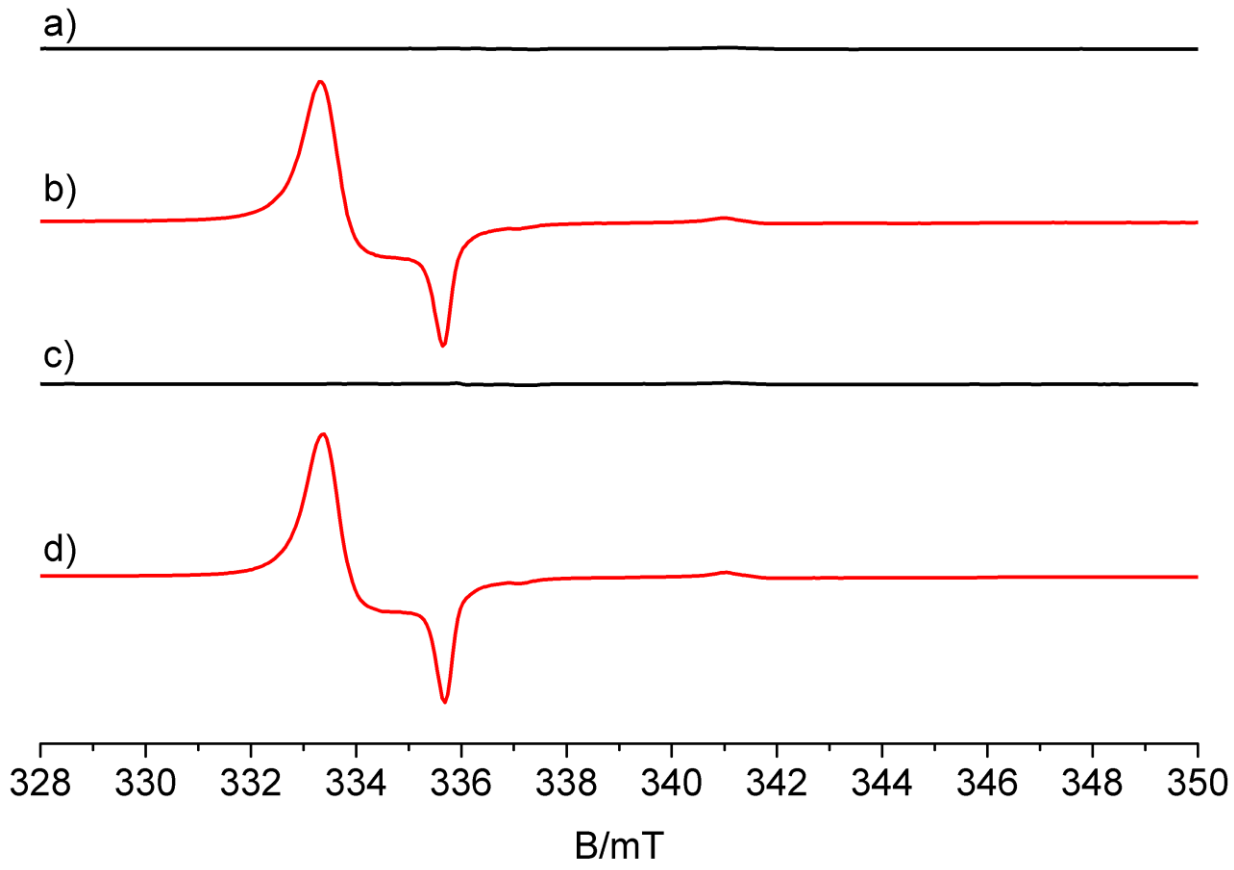

Figure 4: EPR spectra of the Ce05-ZT sample in various conditions. a) as prepared material under vacuum b) in presence of 2 mbar of O_2 c) after outgassing d) after re-adsorption of 2 mbar of O_2.

At the end of the activation procedure described in the experimental section, recording the EPR spectra under vacuum, no signal of relevant paramagnetic centres in the solid is observed, except for a very weak trace of Zr^{3+} centres indicated in the following figures by a single asterisk. Such centre is a defect of the $ZrTiO_4$ matrix and, for sake of simplicity, it will not further considered in this work.[25,38]

Quite the opposite, recording the EPR spectra of the Ce doped zirconium titanate in oxygen atmosphere at 77 K, an intense EPR signal is observed characterized by a **g** tensor whose principal values are g_1=2.026, g_2=2.023 and g_3=2.012. Figure 3A reports the spectrum obtained for the Ce05-ZT sample in presence of 2 mbar of O_2 and the corresponding computer simulation. Notably, the signal completely disappears removing the oxygen by outgassing the sample at room temperature and appears again if a new dose of oxygen is adsorbed, indicating a full reversibility of the process leading to the formation of such a paramagnetic centre. In Figure 4 the change of the EPR spectrum of Ce05-

ZT in presence of O_2 or under vacuum is reported. Inspection of the figure clearly shows that when O_2 is contacted with the surface of the sample an intense paramagnetic signal shows up (Fig. 4b, same of Fig. 3A). The same signal completely disappears when oxygen is removed by pumping (Fig. 4c) and it is fully recovered dosing oxygen again (Fig. Ad). It is worth to mention also that this behaviour is typical of Ce-containing titanate materials and that it is not observed in the case of the undoped $ZrTiO_4$ matrix. The spectrum reported in figure 3A (and 4b) was recorded at liquid nitrogen temperature (77K). However, a weaker signal of the same type is observed at 273 K and its intensity increases with a progressive decrease of the temperature (see Figure S3). The observed signal can be unambiguously ascribed to a superoxide species interacting with tetravalent cerium ions ($O_2^{\bullet-}$ - Ce^{4+}) as indicated by inspection of the data reported in Table 2 showing the close similarity of the signal reported in figure 3 with those of $O_2^{\bullet-}$ species obtained on Ce-containing materials or on bare CeO_2. The unusual g_3 value, clearly higher than g_e, is the fingerprint of the peculiar role of the spin orbit contribution to the g value of superoxide brought about by the adsorbing Ce ions.[39]

It is worth to recall here that the phenomenon reported in Fig. 4 is quite uncommon, essentially for two reasons. First, the formation of the superoxide adduct is fully reversible suggesting that the activation energy is very small for both adsorption and desorption steps. In most cases of superoxide formation the desorption step shows, in fact, a high activation energy due to the high strength of the superoxide-surface bonding. Second, the formation of adsorbed $O_2^{\bullet-}$ occurs, by simple contact between O_2 and the pristine surface with no need of prereduction of the solid. (as in the cases of heterogeneous catalysts for selective oxidation[40] or of photoactivation as in the case of photocatalysis.[41] The phenomenon here described is therefore reminiscent of the chemistry of the so called oxygen carriers that are usually molecular compounds [5-678] and only seldom solid systems.[19-21] To better clarify this point, In Fig. 3B and 3C we report the result of the interaction of O_2 with Ce-$ZrTiO_4$ (Ce05-ZT sample) under irradiation (3B) or with the same material pre-reduced by thermal anneling under vacuum (3C).

substrate	g_1	g_2	g_3	^{17}O hfc-1 (mT)	^{17}O hfc-2 (mT)	^{17}O hfc-3 (mT)	Reference
Ce-$ZrTiO_4$	2.026	2.023	2.012	~ 0	-7.6	~ 0	This work
Superoxide on Ce-containing materials							
CeO_2-TiO_2	2.025	2.021	2.013	unresol.	7.5	unresol.	[21]
CeO_2-TiO_2	2.026	2.021	2.013	unresol.	7.6	unresol.	[21]
CeO_2-TiO_2	2.026	2.018	2.011	-	-	-	[42]
Pt-CeO_2-Al_2O_3	2.028	2.026	2.012	-	-	-	[43]
CeO_2-Cl	2.026	2.022	2.012	unresol.	7.4	unresol.	[44]
CeO_2-SiO_2	2.028	2.016	2.011	< 1.0	7.5	< 0.5	[39]
Superoxide on bare CeO_2							
CeO_2	2.031	2.019	2.011	unresol.	7.5	unresol.	[23]
CeO_2	2.031	2.018	2.011	-	-	-	[45]
CeO_2	2.037	2.014	2.011	-	-	-	[45]
Superoxide on metal oxide							
ZrO_2	2.032-34	2.009	2.003				[46]
TiO_2	2.019-24	2.011	2.005	unresol.	7.6	unresol.	[47]
MgO	2.077	2.008	2.002	0.83	7.6	0.72	[48]
ZnO	2.04-05	2.009	2.002	1.5	8.0	0	[49]
SnO_2	2.024	2009	2.004	unresol.	8.1	unresol.	[50]

Table 2: Spin Hamiltonian parameters of $O_2^{\bullet-}$ species on different substrates.

In the former case, a further contribution to the superoxide intensity occurs due to photoformed superoxide ions generated by UV light excitation, charge separation and electron transfer (eq.s 2 and 3)

$$Ce\text{-}ZrTiO_4 + h\nu \rightarrow e^-_{(CB)} + h^+_{(VB)} \quad (2)$$

$$O_2 + e^- + Ce^{4+} \rightarrow O_2^{\bullet-}/Ce^{4+} \quad (3)$$

Figure 3B clearly shows that irradiation causes the formation of a supplementary dose of adsorbed superoxide as indicated by the intensity of the signal (about twice, Figure S4) and by the slight modification of the spectral shape (compare spectra in figure 3A and 3B). This modification is essentially due to the formation of $O_2^{\bullet-}$ adducts adsorbed on Ti^{4+} and Zr^{4+} surface ions that are not present in the former spectrum (Figure 4A) and that (since are not desorbed by pumping off the gas)

show up after removal of the gas phase (red trace in Figure 4B). As mentioned before in the case of UV light exposed sample, the intensity of $O_2^{\bullet-}$- Ce^{4+} adduct is about twice than that observed after a simple absorption in dark, (see S.I.) This indicate that, because of the contribution of the photo excited electrons, new absorption sites involving Ce ions are generated and the O_2 absorption on these new Ce sites is again fully reversible since the related signal completely vanish after outgassing.. The intensity of the signals of $O_2^{\bullet-}$ on Ti^{4+} and Zr^{4+} (non reversible adsorption) is nearly negligible (caption of Figure 3).

A similar result was obtained by contacting oxygen on a previously annealed sample (Figure 3C). This is due to the role of excess electrons, consequence of the lattice oxygen depletion occurring at high temperature in agreement with the process described by reaction 1. The intensity of the whole superoxide signal is, in this case, much higher (between one and two order of magnitudes) than that of the signals in Figure 3A and 3B. The effect of the reductive annealing therefore is the creation of a large amount of sites for superoxide adsorption. Also in this case by outgassing the sample, the $O_2^{\bullet-}$ -Ce^{4+} adduct completely disappears while the signals due to minor amounts of Zr^{4+}-$O_2^{\bullet-}$ and Ti^{4+}-$O_2^{\bullet-}$ (buried in the main signal) become clearly visible.

To conclude an activated Ce-$ZrTiO_4$ material reversibly adsorbs oxygen, under the form of $O_2^{\bullet-}$, on cerium (IV) ions (Figure 3A). The phenomenon is enhanced if more electrons became available either by UV irradiation (Figure 3B) of by prereduction of the solid (Figure 3C). Beyond any doubt the process here described can be written as

$$Ce^{3+} + O_2 \text{ (gas)} \leftrightarrows Ce^{4+}\text{-}O_2^{\bullet-} \qquad (4)$$

The most striking features of the observed phenomenon are:

a) The adsorption with surface electron transfer is pressure dependent and fully reversible. As discussed before the introduction the reversibility of superoxide formation on oxides is highly uncommon.

b) The surface of the activated material still contains, after a thorough oxidation at high temperature, a consistent number of reduced (Ce^{3+}) centres responsible for the reversible O_2 adsorption. This

confirms the finding obtained by XPS and indicates an interesting, unexpected peculiarity of the investigated solid *e.g.* the property of stabilizing the dopant in its trivalent form generating, in this way, a highly defective solid.

3.2.2 Spin density distribution in the $O_2^{\bullet-}$-Ce^{4+} adduct.

A further characterization of the reversibly adsorbed superoxide species at the Ce-$ZrTiO_4$ surface comes from the spectrum recorded using ^{17}O enriched oxygen (Figure 5). The hyperfine structure, due to the nuclear spin (I = 5/2) of the ^{17}O isotope, indeed, provides indications about the structure of the adsorbed $O_2^{\bullet-}$ and about the spin density distribution. Figure 4 reports the spectrum obtained for the Ce05-ZT sample under 10^{-2} mbar of O_2 enriched with ^{17}O (99% atoms) and the corresponding computer simulation. The hyperfine structure, due to the prevailing presence of the ^{17}O–^{17}O isotopomer, is based on a 11-line structure centred at $g_2 = 2.0229$ and separated by $A_2 = 7.6$ mT (the other components are approximately zero). The structure of this signal clearly indicates the presence of two magnetically equivalent oxygen atoms in the superoxide species adsorbed on Ce^{4+}, thus, the $O_2^{\bullet-}$ complex is a symmetric side-on adduct. The spin density on the atom of the oxygen can be derived from the hyperfine matrix A (Table 2) according to:

$$\boldsymbol{A} = \begin{vmatrix} A_1 & 0 & 0 \\ 0 & A_2 & 0 \\ 0 & 0 & A_3 \end{vmatrix} = a_{iso} + \begin{vmatrix} 2B & 0 & 0 \\ 0 & -B & 0 \\ 0 & 0 & -B \end{vmatrix} \cong 2.5 + \begin{vmatrix} 5.0 & 0 & 0 \\ 0 & -2.5 & 0 \\ 0 & 0 & -2.5 \end{vmatrix} \qquad (5)$$

Where a_{iso} is the Fermi contact term (proportional to the electron spin density in the nuclear volume) and $\boldsymbol{B}$ is the dipolar matrix having the typical form of the electron-nucleus dipolar interaction for an electron in a p orbital (i.e., *2B*, *-B*, *-B*), both expressed in millitesla (mT). Comparing the experimental values with the corresponding atomic value $B°$= 5.15 mT and $A°$=166.0mT, the spin density on the oxygen molecule can be calculated by comparison of the experimental values with the corresponding atomic value ($\rho(2p) = 2B/B°$, $\rho(2s) = a_{iso}/A°$). It thus results that almost of the total spin density is mainly localized (0.98) on a O 2p orbital while the isotropic Fermi contact term indicates a negligible amount of electron spin density (0.015) on the 2s orbital. Such a value of hyperfine coupling and the

corresponding spin density (see table 2) are almost identical to the values obtained on other oxide surfaces where the superoxide species is, however, obtained via non reversible electron transfer.[47,48,49,50] It must be emphasized therefore the novelty of the present results, since the observed superoxide moiety has features clearly similar to those of the vast majority of similar species reported in the literature (side on geometry, complete electron transfer to O_2) but it shows a pressure dependent, totally reversible adsorption similar to that of homogeneous and heterogeneous oxygen carriers that have a very different structure (end on, bent M-O-O structure).

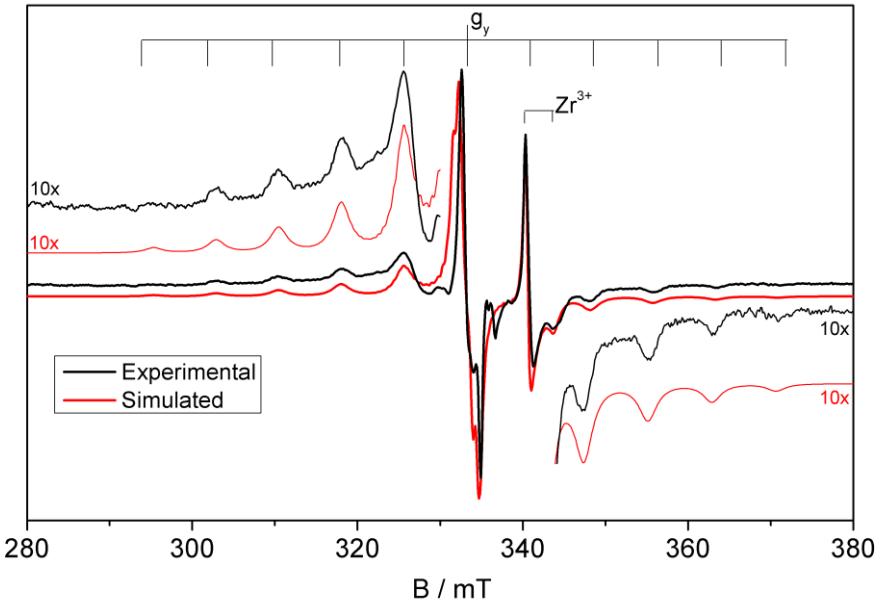

Figure 5: Experimental and simulated EPR spectra of Ce05-ZT sample contacted with $^{17}O_2$ (99% atoms)

3.3 Quantitative evaluation of adsorbed superoxide.

In order to evaluate the adsorption ability of the materials and to perform a quantitative analysis of the amount of adsorbed $O_2^{\bullet-}$ species, EPR spectra of Ce0.5-ZT and Ce10-ZT samples have been recorded at increasing oxygen pressure. In these experiments oxygen is contacted with the sample at RT till the desired equilibrium pressure. The temperature is then lowered to 77 K to record the $O_2^{\bullet-}$ EPR spectrum. The pressure reported in the diagram (Figure 6) refers to the RT value. The integrated area of each EPR signal has been compared with that of a standard solution of 2,2-Di(4-tert-octylphenyl)-1-picrylhydrazyl (DPPH) in cyclohexane in order to estimate the number of $O_2^{\bullet-}$ radical

ions adsorbed on the material. In Figure 6 the number of moles of adsorbed oxygen per gram of sample is reported as a function of oxygen pressure.

Examining the results of Figure 6 (a sort of EPR-based adsorption isotherm) it results that in the case of Ce10-ZT the whole adsorption is almost ten times higher than that of Ce0.5-ZT, indicating, as in the case of the as prepared samples, that the amount of adsorbed oxygen is related to the amount of Ce ions present in the material. In both cases the amount of adsorbed O_2 increases with increasing the oxygen pressure until reaching a plateau. At the highest pressure value, the adsorbed amount apparently decreases. The decrease is only apparent as the EPR signal is affected by the effect of dipolar broadening caused by the interaction between the adsorbed superoxide and the (paramagnetic) oxygen molecules in the physisorbed layer which becomes relevant at higher pressure. From this point the integration of the EPR signal is no longer representative of the true amount of adsorbed O_2.

The results obtained for Ce05-ZT reproduce a Langmuir adsorption model because they can be linearized using the equation (Figure 7):

$$p/n = 1/(K_{eq} * n_m) + p/n_m \qquad (6)$$

Where n_m is the number of moles adsorbed at full coverage, K_{eq} of the surface reaction is the equilibrium constant, p is the pressure and n is the number of adsorbed moles.

In the case of Ce05-ZT the values of the two parameters are $n_m = 2.59 \cdot 10^{-8}$ mol/g and $K_{eq} = 40.4$ respectively.

The Gibbs free energy of the process is -2.4 kJ/mol.

The negative value of ΔG^0 confirms that the formation of superoxide species is a spontaneous process. Its low absolute value is in agreement with the reversibility of the phenomenon.

The O_2 adsorption on Ce10-ZT doesn't follow a Langmuir adsorption model since its isotherm cannot be linearized according to equation 6. Langmuir's model involves the presence of a unique family of isolated, non-interacting adsorption sites. The non-Langmuir trend of the Ce10-ZT isotherm could be due to the presence of various families of sites (heterogeneity of the surface) and to their higher concentration.

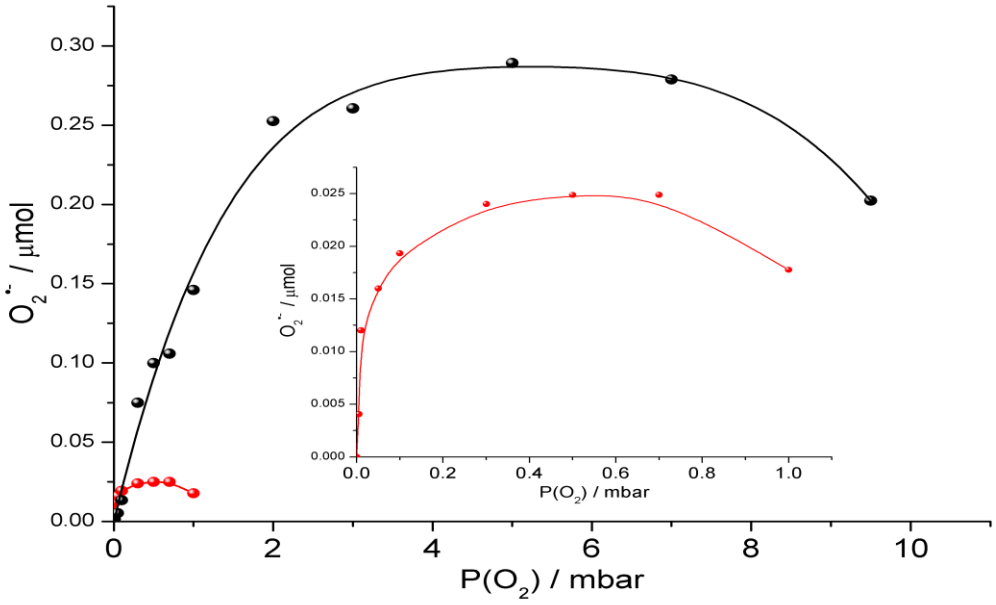

Figure 6: EPR-derived adsorption isotherms of $O_2^{\bullet-}$ on Ce10-ZT (black line) and Ce05-ZT (red line) samples. The absorbed amount was evaluated via double integration of the superoxide spectra. The inset shows the magnification of the Ce05-ZT curve.

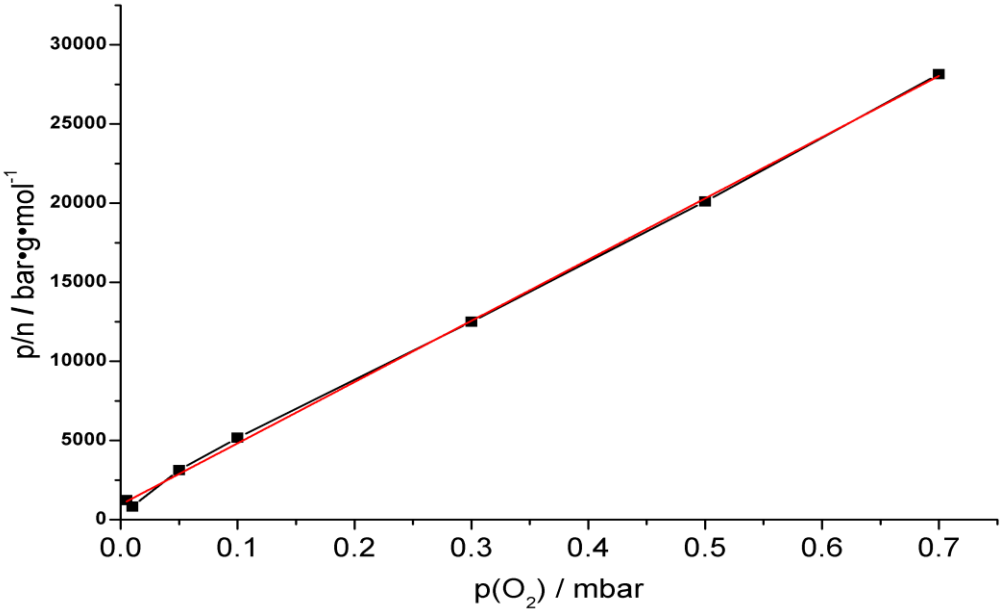

Figure 7: Linearization according to Langmuir isotherm of Ce05-ZT sample

4 Discussion.

The experimental results here reported clearly show that Ce-doped $ZrTiO_4$ material is able to reversibly adsorb O_2 and that this peculiar reactivity is related to the reversible transition of surface Ce ions from reduced (Ce^{3+}) to oxidized (Ce^{4+}) states in presence of adsorbed O_2 (equation 4).

This assumption is based on the EPR parameters of the adsorbed superoxide (typical of interaction with Ce^{4+} ions and is corroborated by two further evidences: i) Ce^{3+} centres are present at the surface even after an highly oxidative treatment as shown by the XPS experiments, ii) the amount of $O_2^{\bullet-}$-Ce^{4+} adduct is proportional to the Ce content of the material (Fig. 6). In fact, when the content of Ce^{3+} with respect to the equilibrium composition of the solid is increased by effect of irradiation or by reductive annealing the amount of adsorbed superoxide dramatically increases. The reversibility of the electron transfer reaction is strictly related to the nature of the cerium based adsorption sites. When O_2^- is adsorbed on different surface ions (namely Zr^{4+} or Ti^{4+}) the adsorbed species is not desorbed outgassing the solid. Scheme 1 summarizes the described $O_2^{\bullet-}$- M^{4+} adduct formation mechanisms (where the M indicates a generic surface cation) highlighting the differences occurring in the case of O_2 adsorption on Ce^{3+} ions respect to the adsorption on titanium or zirconium minority sites.

The observed results allow a preliminary description of the solid prepared doping zirconium titanate with respect to those obtained doping the two parent oxides (ZrO_2 and TiO_2). In Ce- doped ZrO_2, cerium ions are easily hosted in the zirconia matrix by a simple cation substitution due to the structural analogy of the two oxides (both with wurtzite type structure) that favours the dissolution and in spite of the non-negligible difference in size between Zr and Ce ions [28]

The same does not apply in the case of $ZrTiO_4$ (scrutinyite structure, octahedral coordination of Me^{4+} ions more similar to that of TiO_2). Both the different ionic size of the cations and the different structural features of CeO_2 and $ZrTiO_4$ are such to allow a forecast of no (or little) mutual solubility. This is, in fact, what it is usually observed in the case of CeO_2 and TiO_2 that do not form a solid solution but a single mixed compound with a different structure by reaction at high temperature (see before).[21] The results here presented go in the opposite direction and unambiguously indicate that that the solubility of Ce ions in zirconium titanate is similar to that reported for the same ions in ZrO_2. However, the system does not simply accept an ionic substitution (Ce^{4+} for Zr^{4+} or, less probably, Ti^{4+}) but induce a valence alteration in the solid. According to the treatment undergone by the solid

a fraction of cerium is hosted as Ce^{3+} (bigger than Ce^{4+}). This fraction is relatively abundant (40% - 50%) even after a strong oxidative treatment as indicated by the XPS results (see Table 1). The presence of trivalent Ce ions must be compensated for reasons of electric neutrality. This is done by creation of oxygen vacancies as described in section 3.1. We can conclude therefore that the introduction of Ce ions in the lattice of $ZrTiO_4$ creates a solid showing two kinds of Ce ions (Ce^{3+} and Ce^{4+} in variable ratio strongly dependent on the treatment) and a number of oxygen vacancies (V_o). A fraction of Ce^{3+} ions is exposed at the solid surface and is active in oxygen adsorption. Very likely also some oxygen vacancies (whose amount is one half that of Ce^{3+}) are simultaneously exposed at the surface, so that it cannot be excluded that the special site producing reversible oxygen adsorption with total electron transfer to the adsorbate could be built up by the association of a reduced Ce^{3+} ions and the oxygen vacancy. Further investigation, and, possibly, theoretical calculations are thus necessary to define a model able to fully describe the phenomenon.

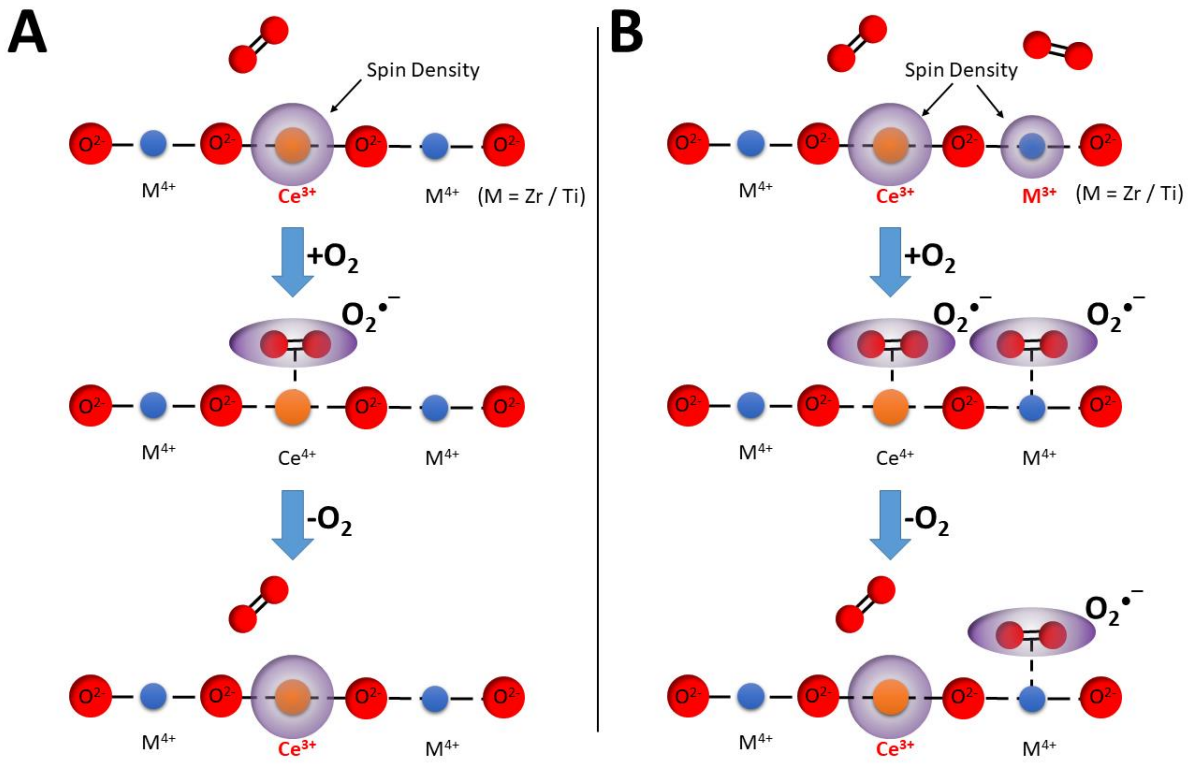

Scheme 1: Evolution of the umpired electron spin density during O_2 adsorption/desorption. A) Ce-doped $ZrTiO_4$. A) Ce-doped $ZrTiO_4$ in presence of excess electrons generated via UV light irradiation or thermal annealing.

5 Conclusions.

Ce-doped $ZrTiO_4$ material is able to reversibly adsorb O_2 in the form of superoxide species ($O_2^{\bullet-}$) and this peculiar reactivity is strictly related to the reversible transition of surface Ce ions from reduced (Ce^{3+}) to oxidized (Ce^{4+}) states. The $O_2^{\bullet-}$ species is adsorbed in side-on geometry and the spin density is close to the unity indicating that the involved electrons are fully transferred during the process. The investigated material is, as far as the Ce ions are concerned, a mixed valence solid with a variable, thought always high, content of Ce^{3+}. The latter parameter can be enhanced by irradiation or, alternatively, by thermal reductive annealing (Fig. 3B and C) reaching rather high values which directly correspond to high oxygen uptakes. The data reported in this work indicates therefore that Ce-doped $ZrTiO_4$ represents a potential material for application in adsorption and separation of O_2 containing gas mixtures. Experimental activities are presently carried out in our laboratory to verify the potential of the investigated systems in practical applications for gas mixtures separation.

Acknowledgments

The work has been supported by the Italian MIUR through the PRIN Project 2015K7FZLH SMARTNESS "Solar driven chemistry: new materials for photo– and electro–catalysis".

References.

[1] O. Carp, C. L. Hiusman, A. Reller, Prog. Solid stese Chem. 32 (2004) 33-177.

https://doi.org/10.1016/j.progsolidstchem.2004.08.001

[2] D. Widmann, R. J. Behm, Acc. Chem. Res. 47 (2014) 740–749.

https://pubs.acs.org/doi/10.1021/ar400203e

[3] M. Fua, X. Yuea, D. Yea, J. Ouyanga, B. Huanga, J. Wua, H. Liangc, Cat. Today 153 (2010) 125–132.

https://doi.org/10.1016/j.cattod.2010.03.017

[4] Y. Wei, J. Liu, Z. Zhao, A. Duan, G. Jiang, C. Xu, J. Gao, H. Heb, X. Wang, Energy Environ. Sci. 4 (2011) 2959-2970. https://doi.org/10.1039/C0EE00813C

[5] J-R. Li, J. Sculley, H-C. Zhou, Chem. Rev. 112 (2012) 869–932. https://doi.org/10.1021/cr200190s

[6] F. Tian, X. Zhang , Y. Chen, RSC Adv., 6 (2016) 31214-31224. https://doi.org/10.1039/C5RA23888A

[7] E. C. Niederhoffer, J. H. Timmons, A. E. Martell, Chem. Rev. 84 (1984) 137-203. https://doi.org/10.1021/cr00060a003

[8] R. D. Jones, D. A. Summerville and F. Basolo, Chem. Rev. 79 (1979) 139–179. https://doi.org/10.1021/cr60318a002

[9] A.T. Gallagher, J.Y. Lee, V. Kathiresan, J.S. Anderson, B.M. Hoffman, T.D. Harris, Chem. Sci. 9 (2018) 1596-1603. https://doi.org/10.1039/C7SC03739B

[10] J. Halpern, B.L. Goodall, G.P. Khare, H.S. Lim, J.J. Pluth, j.A. Pluth, J. Am. Chem. Soc. 97 (1975) 2301-2303. https://doi.org/10.1021/ja00841a068

[11] B.M. Hoffman, D.L. Diemente, F. Basolo, J Am. Chem Soc. 92 (1970) 61-65. https://doi.org/ 10.1021/ja00704a010

[12] R.J. Taylor, R.S. Drago, J.E. George, J. Am. Chem. Soc. 111 (1989) 6610-6615. https://doi.org/10.1021/ja00199a020

[13] P.D. Southon, D.J. Price, P.K. Nielsen, C.J. McKenzie, C.J. Kepert, J. Am. Chem. Soc. 133 (2011) 10885–10891. https://doi.org/ 10.1021/ja202228v

[14] G. Saracco, S. Vankova, C. Pagliano, B. Bonelli, E. Garrone, Phys. Chem. Chem. Phys. 16 (2014) 6139-6145. https://doi.org/ 10.1039/c3cp54896a

[15] D.J. Xiao, M.I. Gonzalez, L.E. Darago, K.D. Vogiatzis, E.l Haldoupis, L. Gagliardi, J.R. Long, J. Am. Chem. Soc. 138 (2016) 7161−7170. https://doi.org/ 10.1021/jacs.6b03680

[16] E.D. Bloch, W.L. Queen, M.R. Hudson, J.A. Mason, D.J. Xiao, L.J. Murray, R. Flacau, C.M. Brown, J.R. Long. Angew. Chem. Int. Ed. 55 (2016) 8605 –8609. https://doi.org/ 10.1002/anie.201602950

[17] J.S. Anderson, A.T. Gallagher, J.A. Mason, T.D. Harris, J. Am. Chem. Soc. 136 (2014) 16489−16492. https://doi.org/ 10.1021/ja5103103

[18] L.J. Murray, M. Dinca, J. Yano, S. Chavan, S. Bordiga, C.M. Brown, Jeffrey R. Long. J. Am. Chem. Soc. 132 (2010) 7856–7857. https://doi.org/ 10.1021/ja1027925

[19] E. Giamello, Z. Sojka, M. Che, A. Zecchina, J. Phys. Chem. 1986, 90, 6084-6060. https://doi.org/10.1021/j100281a008

[20] Z. Sojka, E. Giamello, M. Che, A. Zecchina, K. Dyrek, J. Phys. Chem. 92, (1988) 1541-1547. https://doi.org/10.1021/j100317a034

[21] C. Gionco, E. Giamello, L. Mino, M.C. Paganini, Phys. Chem. Chem. Phys. 2014, 16, 21438-21445. https://doi.org/0.1039/c4cp03195d

[22] M. Gideoni, M. Steinberg. J. Solid State Chem. 4 (1972) 370-373. https://doi.org/10.1016/0022-4596(72)90151-X

[23] M. Gideoni, N. Kautherr, M. Steinberg, An ESR Study of $^{17}0_2$ on Cerium(IV) Oxide. Isr. J. Chem. 12 (1974) 1069-1073. https://doi.org/10.1002/ijch.197400102

[24] N. Siedl, P. Gügel, O. Diwald, J. Phys. Chem. C 117 (2013) 20722−20729. https://doi.org/ org/10.1021/jp4069834

[25] V. Polliotto, E. Albanese, S. Livraghi, P. Indyka, Z. Sojka, G. Pacchioni, E. Giamello, J. Phys. Chem. C 121 (2017) 5487-5497. https://doi.org/10.1021/acs.jpcc.6b12892

[26] L. Lutterotti, S. Matthies, H.R. Wenk, A. S. Schultz and J. W. Richardson, J. Appl. Phys. 81 (1997) 594-600.

[27] http://maud.radiographema.com

[28] M. Alifanti, B. Baps, N. Blangenois, J. Naud, P. Grange, and B. Delmon, Chem. Mater. 15 (2003) 395-403. https:// doi.org/10.1021/cm021274j

[29] V. Polliotto, E. Albanese, S. Livraghi, S. Agnoli, G, Pacchioni, E. Giamello, Cat. Today *in press.* https://doi.org/10.1016/j.cattod.2018.09.026

[30] P. Burroughs, A. Hamnet, A.F. Orchard, G. Thornton, J. Chem. Soc. Dalton. 0 (1976) 1686-1698. https://doi.org/10.1039/DT9760001686

[31] A. Fujimori, Phys. Rev. B 28 (1983) 2281-2283. https://doi.org/10.1103/PhysRevB.28.2281

[32] L. Artiglia, S. Agnoli, M. C. Paganini, M. Cattelan, G. Granozzi, ACS Appl. Mater. Interfaces. 6 (2014) 20130-20136. https://doi.org/10.1021/am5057129

[33] B.M. Reddy, A. Khan, Y. Yamada, T. Kobayashi, S. Loridant, J-C. Volta J. Phys. Chem. B 107 (2003) 11475-11484. https://doi.org/10.1021/jp0358376

[34] S. Benkoula, O. Sublemontier, M. Patanen, C. Nicolas, F. Sirotti, A. Naitabdi, F. Gaie-Levrel, E.Antonsson, D. Aureau, F-X. Ouf, S-I. Wada, A. Etcheberry, K. Ueda, C. Miron Sci. Reports 5 (2015) 15088. https://doi.org/10.1038/srep15088

[35] L. Artiglia A. Borg, E.M.J. Johansson, S. Plogmaker, H. Rensmo, P. Uvdal, A. Sandell, J. Phys. Chem. C, 116 (2012) 12532–12540 https://doi.org/10.1021/jp111335w

[36] L. Soler, A. Casanovas, C. Escudero, V. Pérez-Dieste, E. Aneggi, A. Trovarelli, J. Llorca ChemCatChem 8 (2016) 2748 – 2751. https://doi.org/10.1002/cctc.201601038

[37] B. Eren, C. Heine, H. Bluhm, G. A. Somorjai, M. Salmeron, J. Am. Chem. Soc. 137 (2015) 11186–11190. https://doi.org/ 10.1021/jacs.5b07451

[38] V. Polliotto, E. Albanese, S. Livraghi, G. Pacchioni, E. Giamello,. J. Mat. Chem. A. 5 (2017) 13062-13071. https://doi.org/10.1039/c7ta03047a

[39] M. Che, J.F.J. Kibblewh, A.J. Tench, M. Dufaux, C. Naccache, J. Chem. Soc., Faraday Trans. 69 (1973) 857-863. https://doi.org/10.1039/F19736900857

[40] M. Anpo, M. Che, B. Fubini, E. Garrone, E. Giamello, M.C. Paganini, Top. Catal. 8 (1999) 189-198. https://doi.org/10.1023/A:101911732

[41] G. Barolo, S. Livraghi, M. Chiesa, M. C. Paganini, E. Giamello, J. Phys. Chem. C 116 (2012) 20887 − 20894.https://doi.org/10.1021/jp306123d

[42] J.M. Coronado, A.J. Maira, A. Mart´ınez-Arias, J.C. Conesa, J. Soria, J. Photochem. Photobiol. A: Chemistry 150 (2002) 213–221. https://doi.org/10.1016/S1010-6030(02)00092-8

[43] J. Soria, A. Martinez-Arias, J.M. Coronado, J.C. Conesa, Colloids Surf., A 115 (1996) 215-221. https://doi.org/10.1016/0927-7757(96)03611-4

[44] J. Soria, J.C. Conesa, A. Martı´nez-Arias, Colloids Surf., A 158 (1999) 67–74. https://doi.org/10.1016/S0927-7757(99)00132-6

[45] X. Zhang, K. J. Klabunde, Inorg. Chem. 31 (1992) 1706-1709. https://doi.org/10.1021/ic00035a034

[46] S. Livraghi, F. Olivero, M. C. Paganini, E. Giamello, J. Phys. Chem. C 114 (2010) 18553–18558. https://doi.org/10.1021/jp106241c

[47] E. Carter, A.F. Carley, D.M. Murphy, J. Phys. Chem. C 111 (2007) 10630-10638. https://doi.org/10.1021/jp0729516

[48] M. Chiesa, E. Giamello, M.C. Paganini, Z. Sojka, D.M. Murphy, J. Chem. Phys. 116 (2002) 4266-4274. https://doi.org/10.1063/1.1447907

[49] A. J. Tench, T. Lawson, Chem. Phys. Lett. 8 (1971) 177-178. https://doi.org/10.1016/0009-2614(71)80007-6

[50] P. Meriaudeau, C. Naccache, A.J. Tench, J. Cat. 21 (1971) 208-2011. https://doi.org/10.1016/0021-9517(71)90139-4